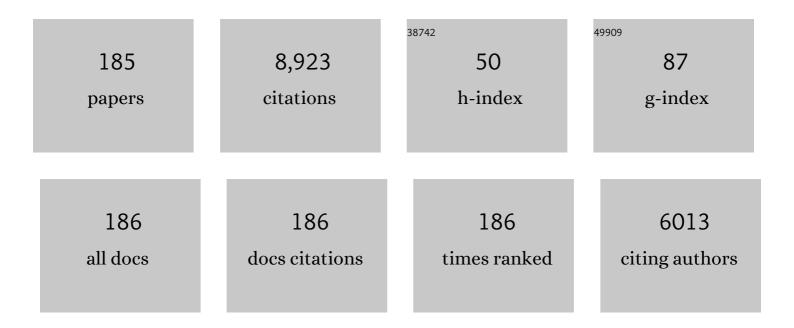
List of Publications by Year in descending order

Source: https://exaly.com/author-pdf/562243/publications.pdf Version: 2024-02-01



Ριινμιά Ελν

#	Article	IF	CITATIONS
1	Low-frequency plasmonic state and tunable negative permittivity in percolative graphite / barium titanate composites. Ceramics International, 2022, 48, 832-836.	4.8	12
2	Synthesis of carbon/SiO2 core-sheath nanofibers with Co-Fe nanoparticles embedded in via electrospinning for high-performance microwave absorption. Advanced Composites and Hybrid Materials, 2022, 5, 513-524.	21.1	89
3	Ultraweakly and fine-tunable negative permittivity of polyaniline/nickel metacomposites with high-frequency diamagnetic response. Composites Science and Technology, 2022, 217, 109092.	7.8	35
4	Metallic Ferromagnet of La _{0.5} Sr _{0.5} MnO ₃ with Negative Permittivity and Permeability. Advanced Electronic Materials, 2022, 8, 2101020.	5.1	7
5	Defect-induced insulator-metal transition and negative permittivity in La1-Ba CoO3 perovskite structure. Journal of Materials Science and Technology, 2022, 112, 77-84.	10.7	38
6	Nickel/yttrium iron garnet metacomposites with adjustable negative permittivity behavior toward electromagnetic shielding application. Composites Part A: Applied Science and Manufacturing, 2022, 155, 106842.	7.6	19
7	Flexible multi-walled carbon nanotubes/polyvinylidene fluoride membranous composites with weakly negative permittivity and low frequency dispersion. Composites Part A: Applied Science and Manufacturing, 2022, 156, 106854.	7.6	34
8	Epsilon-negative behavior and its capacitance enhancement effect on trilayer-structured polyimide–silica/multiwalled carbon nanotubes/polyimide–polyimide composites. Journal of Materials Chemistry C, 2022, 10, 4286-4294.	5.5	12
9	Facile and Efficient Negative Permittivity Realization of Copper Microwire Polymer Metacomposites at X-Band Frequency. Journal of Electronic Materials, 2022, 51, 2107-2113.	2.2	4
10	Two-dimensional Ti3C2Tx/carbonized wood metacomposites with weakly negative permittivity. Advanced Composites and Hybrid Materials, 2022, 5, 2369-2377.	21.1	24
11	Synergistic effect of dielectric resonance and plasma oscillation on negative permittivity behavior in La1-Sr MnO3 single-phase ceramic. Ceramics International, 2022, 48, 8417-8422.	4.8	7
12	Negative permittivity behavior of carbon fibre/alumina ceramic composites prepared by hot-press sintering. Ceramics International, 2022, 48, 10031-10038.	4.8	14
13	Coassembly of elastomeric microfibers and silver nanowires for fabricating ultra-stretchable microtextiles with weakly and tunable negative permittivity. Composites Science and Technology, 2022, 223, 109415.	7.8	29
14	Dielectric enhancement effect in biomorphic porous carbon-based iron@iron carbide â€~meta-powder' for light-weight microwave absorption material design. Advanced Composites and Hybrid Materials, 2022, 5, 3176-3189.	21.1	36
15	Recent advances in radio-frequency negative dielectric metamaterials by designing heterogeneous composites. Advanced Composites and Hybrid Materials, 2022, 5, 679-695.	21.1	168
16	Concurrently Achieving High Discharged Energy Density and Efficiency in Composites by Introducing Ultralow Loadings of Core–Shell Structured Graphene@TiO ₂ Nanoboxes. ACS Applied Materials & Interfaces, 2022, 14, 29292-29301.	8.0	17
17	Epsilon-near-zero response derived from collective oscillation in the metacomposites with ultralow plasma frequency. Composites Science and Technology, 2022, 227, 109600.	7.8	20
18	Flexible and biocompatible poly (vinyl alcohol)/multi-walled carbon nanotubes hydrogels with epsilon-near-zero properties. Journal of Materials Science and Technology, 2022, 131, 91-99.	10.7	22

#	Article	IF	CITATIONS
19	Doped ceramics of indium oxides for negative permittivity materials in MHz-kHz frequency regions. Journal of Materials Science and Technology, 2021, 61, 125-131.	10.7	106
20	TiN/Al2O3 binary ceramics for negative permittivity metacomposites at kHz frequencies. Journal of Alloys and Compounds, 2021, 855, 157499.	5.5	60
21	TiN/CaCu3Ti4O12 binary ceramics with tunable and weakly negative permittivity. Materials Letters, 2021, 283, 128824.	2.6	7
22	Recent developments on epoxy-based syntactic foams for deep sea exploration. Journal of Materials Science, 2021, 56, 2037-2076.	3.7	29
23	Significantly enhanced dielectric permittivity and low loss in epoxy composites incorporating 3d W-WO3/BaTiO3 foams. Journal of Materials Science, 2021, 56, 4254-4265.	3.7	60
24	Low-frequency plasmonic state and negative permittivity in copper/titanium dioxide percolating composites. Ceramics International, 2021, 47, 2208-2213.	4.8	22
25	Optimizing the Soft Magnetic Properties of Mn-Zn Ferrite by a Proper Control of Sintering Process. Journal of Electronic Materials, 2021, 50, 1467-1473.	2.2	4
26	Carbon fiber skeleton/silver nanowires composites with tunable negative permittivity behavior. EPJ Applied Metamaterials, 2021, 8, 1.	1.5	3
27	Epsilonâ€Negative Carbon Aerogels with State Transition from Dielectric to Degenerate Semiconductor. Advanced Electronic Materials, 2021, 7, 2000877.	5.1	25
28	Epsilon-negative media from the viewpoint of materials science. EPJ Applied Metamaterials, 2021, 8, 11.	1.5	23
29	Hierarchically porous Co/C nanocomposites for ultralight high-performance microwave absorption. Advanced Composites and Hybrid Materials, 2021, 4, 173-185.	21.1	356
30	Communication—Dielectric Dispersion of Chromium Carbide/Copper Calcium Titanate Metacomposites: Epsilon-Negative, Epsilon-Near-Zero, and Inductive Character. ECS Journal of Solid State Science and Technology, 2021, 10, 023006.	1.8	0
31	Communication—Modulation Mechanism of Epsilon-Negative and Epsilon-Near-Zero Behavior in Carbon Nanotube-Carbon Black/Copper Calcium Titanate Ternary Metacomposites. ECS Journal of Solid State Science and Technology, 2021, 10, 023007.	1.8	3
32	Tailorable epsilon-negative and epsilon-near-zero behavior of TiC/CCTO metacomposites: Low-frequency plasma oscillation. Functional Materials Letters, 2021, 14, 2150015.	1.2	1
33	Negative permittivity behavior in Ti3AlC2-polyimide composites and the regulation mechanism. Journal of Materials Science: Materials in Electronics, 2021, 32, 10388-10397.	2.2	31
34	Improved breakdown strengths and energy storage properties of polyimide composites: The effect of internal interfaces of C/ <scp>SiO₂</scp> hybrid nanoparticles. Polymer Composites, 2021, 42, 3000-3010.	4.6	50
35	Tailoring the electromagnetic properties of perovskite La0.7Sr0.3MnO3 ceramics by Co doping. Journal of Materials Science, 2021, 56, 10183-10190.	3.7	6
36	Percolated cermets of nickel/yttrium iron garnet for double negative metacomposites. Composites Communications, 2021, 24, 100667.	6.3	16

#	Article	IF	CITATIONS
37	Effect of spherical copper particle size on the negative permittivity behavior of copper/polypropane composite. Journal of Materials Science: Materials in Electronics, 2021, 32, 11588-11592.	2.2	1
38	Communication—Tunable Negative Permittivity of Ti3SiC2 MAX Phase Granular Metacomposites. ECS Journal of Solid State Science and Technology, 2021, 10, 043002.	1.8	3
39	Tailorable negative permittivity of graphene-carbon nanotube/copper calcium titanate metacomposites. Ceramics International, 2021, 47, 9971-9978.	4.8	21
40	Effects of Voltage and Temperature on Photoelectric Properties of Rolled-Up Quantum Well Nanomembranes. Journal of Electronic Materials, 2021, 50, 3111-3115.	2.2	1
41	Iron/epoxy random metamaterials with adjustable epsilon-near-zero and epsilon-negative property. Journal of Materials Science: Materials in Electronics, 2021, 32, 15995-16007.	2.2	19
42	Spark plasma sintered GR-CNT/CaCu3Ti4O12 ceramic nanocomposites with tunable epsilon-negative and epsilon-near-zero property. Ceramics International, 2021, 47, 17345-17352.	4.8	13
43	Achieving Concurrent High Energy Density and Efficiency in All-Polymer Layered Paraelectric/Ferroelectric Composites via Introducing a Moderate Layer. ACS Applied Materials & Interfaces, 2021, 13, 27522-27532.	8.0	87
44	Improved magnetic properties of iron-based soft magnetic composites with a double phosphate-SiO2 shells structure. Journal of Materials Science: Materials in Electronics, 2021, 32, 21472-21482.	2.2	9
45	Weakly negative permittivity with an extremely low plasma frequency in polyvinyl alcohol/graphene membranous metacomposites. Journal of Materials Science: Materials in Electronics, 2021, 32, 23081-23089.	2.2	5
46	Negative permittivity behavior in silver nanowire-assisted polyaniline metacomposites induced by the low-frequency plasmonic oscillation. Journal of Materials Science: Materials in Electronics, 2021, 32, 26851-26856.	2.2	0
47	Negative permittivity behavior in carbon fibre/silicon nitride ceramic composites prepared by spark plasma sintering. Ceramics International, 2021, 47, 35201-35208.	4.8	14
48	Radio-frequency epsilon-negative property and diamagnetic response of percolative Ag/CCTO metacomposites. Scripta Materialia, 2021, 203, 114067.	5.2	33
49	Significantly enhanced high permittivity and negative permittivity in Ag/Al2O3/3D-BaTiO3/epoxy metacomposites with unique hierarchical heterogeneous microstructures. Composites Part A: Applied Science and Manufacturing, 2021, 149, 106559.	7.6	54
50	Tailorable high-k and negative-k percolation behaviors in PPy/P(VDF-HFP) composites. Composites Communications, 2021, 28, 100945.	6.3	11
51	Lightweight Fe3C@Fe/C nanocomposites derived from wasted cornstalks with high-efficiency microwave absorption and ultrathin thickness. Advanced Composites and Hybrid Materials, 2021, 4, 1226-1238.	21.1	215
52	Negative permittivity in titanium nitrideâ€alumina composite for functionalized structural ceramics. Journal of the American Ceramic Society, 2020, 103, 403-411.	3.8	69
53	Low-loss and temperature-stable negative permittivity in La0.5Sr0.5MnO3 ceramics. Journal of the European Ceramic Society, 2020, 40, 1917-1921.	5.7	38
54	Design and analysis of negative permittivity behaviors in barium titanate/nickel metacomposites. Acta Materialia, 2020, 185, 412-419.	7.9	154

#	Article	IF	CITATIONS
55	Epsilon-negative behavior of BaTiO3/Ag metacomposites prepared by an in situ synthesis. Ceramics International, 2020, 46, 9342-9346.	4.8	28
56	Tunable negative permittivity behavior and electromagnetic shielding performance of silver/silicon nitride metacomposites. Composites Part A: Applied Science and Manufacturing, 2020, 130, 105753.	7.6	75
57	Flexible and transparent polymer/cellulose nanocrystal nanocomposites with high thermal conductivity for thermal management application. Journal of Applied Polymer Science, 2020, 137, 48864.	2.6	13
58	Fine-tuning of negative permittivity behavior in amorphous carbon/alumina metacomposites. Ceramics International, 2020, 46, 8942-8948.	4.8	14
59	Radio-frequency negative permittivity of carbon nanotube/copper calcium titanate ceramic nanocomposites fabricated by spark plasma sintering. Ceramics International, 2020, 46, 2261-2267.	4.8	36
60	Twoâ€dimensional Ti ₃ C ₂ T _x /poly(vinylidene fluoride) metacomposites with weakly negative permittivity. Polymer Composites, 2020, 41, 1820-1829.	4.6	6
61	Core-shell structured tungsten carbide / polypyrrole metacomposites with tailorable negative permittivity at the radio frequency. Polymer, 2020, 188, 122125.	3.8	13
62	Tunneling-induced negative permittivity in Ni/MnO nanocomposites by a bio-gel derived strategy. Journal of Materials Chemistry C, 2020, 8, 3029-3039.	5.5	169
63	Direct Observation of Stable Negative Capacitance in SrTiO ₃ @BaTiO ₃ Heterostructure. Advanced Electronic Materials, 2020, 6, 1901005.	5.1	26
64	Flexible 2.5D Metamaterial with High Mechanical Bearing Capacity for Electromagnetic Interference Filters at Microwave Frequency. Advanced Engineering Materials, 2020, 22, 1901126.	3.5	7
65	In situ chemoâ€polymerized polypyrroleâ€coated filter paper for highâ€efficient solar vapor generation. International Journal of Energy Research, 2020, 44, 1191-1204.	4.5	22
66	Graphene–Carbon Black/CaCu ₃ Ti ₄ O ₁₂ Ternary Metacomposites toward a Tunable and Weakly ε-Negative Property at the Radio-Frequency Region. Journal of Physical Chemistry C, 2020, 124, 23361-23367.	3.1	30
67	Negative dielectric permittivity and high-frequency diamagnetic responses of percolated nickel/rutile cermets. Composites Part A: Applied Science and Manufacturing, 2020, 139, 106132.	7.6	32
68	Doping-dependent negative dielectric permittivity realized in mono-phase antimony tin oxide ceramics. Journal of Materials Chemistry C, 2020, 8, 11610-11617.	5.5	43
69	Regulation mechanism of metal ions towards magnetic properties in Mn1â^'xZnxFe2O4. Journal of Materials Science: Materials in Electronics, 2020, 31, 22905-22911.	2.2	3
70	Simultaneous epsilon-negative and mu-negative property of Ni/CaCu3Ti4O12 metacomposites at radio-frequency region. Journal of Alloys and Compounds, 2020, 847, 156526.	5.5	25
71	Porous Fe@Fe3O4-C Nanocomposite Using Polyvinyl Alcohol Sponge as Template for Microwave Absorption. Journal of Electronic Materials, 2020, 49, 6394-6402.	2.2	9
72	Fabrication and Study on Thermal Conductivity, Electrical Properties, and Mechanical Properties of the Lightweight Carbon/Carbon Fiber Composite. Journal of Chemistry, 2020, 2020, 1-15.	1.9	1

#	Article	IF	CITATIONS
73	Compressible sliver nanowires/polyurethane sponge metacomposites with weakly negative permittivity controlled by elastic deformation. Journal of Materials Science, 2020, 55, 15481-15492.	3.7	25
74	Polyvinyl alcohol/carbon fibers composites with tunable negative permittivity behavior. Surfaces and Interfaces, 2020, 21, 100735.	3.0	28
75	Weakly negative permittivity with frequency-independent behavior in flexible thermoplastic polyurethanes/multi-walled carbon nanotubes metacomposites. Materials Today Communications, 2020, 24, 101230.	1.9	7
76	Layer-structured BaTiO ₃ /P(VDF–HFP) composites with concurrently improved dielectric permittivity and breakdown strength toward capacitive energy-storage applications. Journal of Materials Chemistry C, 2020, 8, 10257-10265.	5.5	91
77	Ultrahigh discharge efficiency and improved energy density in rationally designed bilayer polyetherimide–BaTiO ₃ /P(VDF-HFP) composites. Journal of Materials Chemistry A, 2020, 8, 5750-5757.	10.3	170
78	Nitrogen-doped carbon nanofibers with sulfur heteroatoms for improving microwave absorption. Journal of Materials Science, 2020, 55, 5832-5842.	3.7	30
79	Flexible multi-walled carbon nanotubes/polydimethylsiloxane membranous composites toward high-permittivity performance. Advanced Composites and Hybrid Materials, 2020, 3, 1-7.	21.1	95
80	Epsilon-negative BaTiO3/Cu composites with high thermal conductivity and yet low electrical conductivity. Journal of Materiomics, 2020, 6, 145-151.	5.7	58
81	Flexible silver nanowire/carbon fiber felt metacomposites with weakly negative permittivity behavior. Physical Chemistry Chemical Physics, 2020, 22, 5114-5122.	2.8	103
82	Dielectric properties of Ag/paper-based metacomposite with sandwich-structure forward low dielectric loss in megahertz frequency range. Journal of Materials Science: Materials in Electronics, 2020, 31, 4245-4252.	2.2	3
83	Tunable radio-frequency negative permittivity of Carbon/CaCu3Ti4O12 metacomposites. Journal of Alloys and Compounds, 2020, 834, 155164.	5.5	30
84	Hydrosoluble Graphene/Polyvinyl Alcohol Membranous Composites with Negative Permittivity Behavior. Macromolecular Materials and Engineering, 2020, 305, 1900709.	3.6	59
85	Communication—Tunable Epsilon-Negative Property in FeCrNi/CaCu ₃ Ti ₄ O ₁₂ Metacomposites. ECS Journal of Solid State Science and Technology, 2020, 9, 053003.	1.8	4
86	Communication—Tunable Epsilon-Negative Property of Nickel/Copper Calcium Titanate Cermets. ECS Journal of Solid State Science and Technology, 2020, 9, 123004.	1.8	4
87	Fabrication of Co/Al2O3 Composite Nanofiber via Electrospinning with Tunable Magnetic Properties. Fibers and Polymers, 2020, 21, 2485-2493.	2.1	6
88	Core–Shell Structural Barium Ferrite/Polypyrrole Nanocomposites with Enhanced Microwave Absorption Properties. Journal of Nanoelectronics and Optoelectronics, 2020, 15, 1312-1320.	0.5	5
89	Weakly negative permittivity and low frequency dispersive behavior in graphene/epoxy metacomposites. Journal of Materials Science: Materials in Electronics, 2019, 30, 14745-14754.	2.2	40
90	Negative permittivity derived from inductive characteristic in the percolating Cu/EP metacomposites. Journal of Materials Science and Technology, 2019, 35, 2463-2469.	10.7	59

#	Article	IF	CITATIONS
91	Preparation and Properties Characterization of Interpenetrating Polymer Networks/Organically Modified Montmorillonite/Scrap Leather Fibers Composites. Fibers and Polymers, 2019, 20, 1958-1968.	2.1	3
92	Facile Synthesis of Fe@Fe ₃ C/C Nanocomposites Derived from Bulrush for Excellent Electromagnetic Wave-Absorbing Properties. ACS Sustainable Chemistry and Engineering, 2019, 7, 18765-18774.	6.7	90
93	Tunable Negative Permittivity in Flexible Graphene/PDMS Metacomposites. Journal of Physical Chemistry C, 2019, 123, 23635-23642.	3.1	178
94	Chiffon cake-derived hierarchically porous carbon with efficient microwave absorption properties. Journal of Materials Science: Materials in Electronics, 2019, 30, 19173-19181.	2.2	12
95	Tunable negative permittivity and magnetic performance of yttrium iron garnet/polypyrrole metacomposites at the RF frequency. Journal of Materials Chemistry C, 2019, 7, 3160-3167.	5.5	82
96	Negative permittivity behavior in percolative molybdenum/alumina composites. Ceramics International, 2019, 45, 16618-16624.	4.8	12
97	Reverse design of negative permittivity property in Nickel-Network/Epoxy composites. Materials Letters, 2019, 248, 177-180.	2.6	4
98	Broadband microwave absorber constructed by reduced graphene oxide/La _{0.7} Sr _{0.3} MnO ₃ composites. RSC Advances, 2019, 9, 41817-41823.	3.6	13
99	Low-temperature sintering Graphene/CaCu3Ti4O12 nanocomposites with tunable negative permittivity. Journal of Alloys and Compounds, 2019, 771, 699-710.	5.5	73
100	Targeted Double Negative Properties in Silver/Silica Random Metamaterials by Precise Control of Microstructures. Research, 2019, 2019, 1-11.	5.7	30
101	Targeted Double Negative Properties in Silver/Silica Random Metamaterials by Precise Control of Microstructures. Research, 2019, 2019, 1021368.	5.7	118
102	Oxygen vacancy derived local build-in electric field in mesoporous hollow Co ₃ O ₄ microspheres promotes high-performance Li-ion batteries. Journal of Materials Chemistry A, 2018, 6, 6967-6976.	10.3	242
103	Silica microsphere templated self-assembly of a three-dimensional carbon network with stable radio-frequency negative permittivity and low dielectric loss. Journal of Materials Chemistry C, 2018, 6, 5239-5249.	5.5	143
104	An overview of metamaterials and their achievements in wireless power transfer. Journal of Materials Chemistry C, 2018, 6, 2925-2943.	5.5	166
105	Functional nano-units prepared by electrostatic self-assembly for three-dimension carbon networks hosted in CaCu3Ti4O12 ceramics towards radio-frequency negative permittivity. Journal of Alloys and Compounds, 2018, 743, 618-625.	5.5	32
106	Tunable negative permittivity and permeability of yttrium iron garnet/polyaniline composites in radio frequency region. Journal of Materials Science: Materials in Electronics, 2018, 29, 6119-6124.	2.2	18
107	Metacomposites: functional design via titanium nitride/nickel(II) oxide composites towards tailorable negative dielectric properties at radio-frequency range. Journal of Materials Science: Materials in Electronics, 2018, 29, 5853-5861.	2.2	16
108	The negative permittivity behavior of carbon nanotubes/yttrium iron garnet composites in the radio frequency. Materials Letters, 2018, 213, 282-285.	2.6	3

#	Article	IF	CITATIONS
109	Carbon aerogels towards new candidates for double negative metamaterials of low density. Carbon, 2018, 129, 598-606.	10.3	105
110	Radioâ€frequency negative permittivity in the graphene/silicon nitride composites prepared by spark plasma sintering. Journal of the American Ceramic Society, 2018, 101, 1598-1606.	3.8	40
111	Strategy of adjusting negative permittivity with invariant permeability property in metallic granular percolating composites. Journal of Materials Science: Materials in Electronics, 2018, 29, 1246-1253.	2.2	8
112	A plasmonic interfacial evaporator for high-efficiency solar vapor generation. Sustainable Energy and Fuels, 2018, 2, 2762-2769.	4.9	53
113	Copper Sulfide-Based Plasmonic Photothermal Membrane for High-Efficiency Solar Vapor Generation. ACS Applied Materials & Interfaces, 2018, 10, 35154-35163.	8.0	107
114	Low loading carbon nanotubes supported polypyrrole nano metacomposites with tailorable negative permittivity in radio frequency range. Organic Electronics, 2018, 63, 362-368.	2.6	12
115	Flexible acrylic-polyurethane/copper composites with a frequency and temperature-independent permittivity. Journal of Materials Science: Materials in Electronics, 2018, 29, 20832-20839.	2.2	7
116	Iron Granular Percolative Composites toward Radio-Frequency Negative Permittivity. ECS Journal of Solid State Science and Technology, 2018, 7, N132-N136.	1.8	4
117	Regulation mechanism of negative permittivity in poly (p-phenylene sulfide)/multiwall carbon nanotubes composites. Synthetic Metals, 2018, 244, 15-19.	3.9	17
118	Hollow nanoporous red phosphorus as an advanced anode for sodium-ion batteries. Journal of Materials Chemistry A, 2018, 6, 12992-12998.	10.3	36
119	Tunable and weakly negative permittivity at radio frequency range based on titanium nitride/polyethylene terephthalate composites. Journal of Materials Science: Materials in Electronics, 2018, 29, 15994-16003.	2.2	10
120	Flexible Polyimide Nanocomposites with dc Bias Induced Excellent Dielectric Tunability and Unique Nonpercolative Negative- <i>k</i> toward Intrinsic Metamaterials. ACS Applied Materials & Interfaces, 2018, 10, 26713-26722.	8.0	47
121	Negative permittivity behavior of titanium nitride/polyphenylene sulfide "metacomposites―under radio frequency. Journal of Materials Science: Materials in Electronics, 2018, 29, 12144-12151.	2.2	9
122	Bio-gel derived nickel/carbon nanocomposites with enhanced microwave absorption. Journal of Materials Chemistry C, 2018, 6, 8812-8822.	5.5	301
123	Nanoporous Red Phosphorus on Reduced Graphene Oxide as Superior Anode for Sodium-Ion Batteries. ACS Nano, 2018, 12, 7380-7387.	14.6	120
124	Magnetic properties and special morphology of barium ferrite via electrospinning. Rare Metals, 2017, 36, 113-117.	7.1	4
125	Electromagnetic attenuation property of multiphase Fe–Fe3O4–Al2O3 cermets near percolation threshold. Rare Metals, 2017, 36, 42-45.	7.1	3
126	An impregnation-reduction method to prepare graphite nanosheet/alumina composites and its high-frequency dielectric properties. Rare Metals, 2017, 36, 205-208.	7.1	3

#	Article	IF	CITATIONS
127	Negative permittivity adjusted by SiO2-coated metallic particles in percolative composites. Journal of Alloys and Compounds, 2017, 725, 1259-1263.	5.5	64
128	Significantly improved dielectric performances of sandwich-structured polymer composites induced by alternating positive-k and negative-k layers. Journal of Materials Chemistry A, 2017, 5, 14575-14582.	10.3	121
129	Dielectric and Magnetic Relaxation Behavior in Fe78Si9B13/Polyaniline Composites at Radio-Frequency Range. ECS Journal of Solid State Science and Technology, 2017, 6, N87-N91.	1.8	0
130	Enhanced permittivity in flexible carbon-fiber and acrylic-polyurethane composites. Materials Letters, 2017, 205, 44-47.	2.6	13
131	Tunable Negative Permittivity with Fano-like Resonance and Magnetic Property in Percolative Silver/Yittrium Iron Garnet Nanocomposites. Journal of Physical Chemistry C, 2017, 121, 7564-7571.	3.1	75
132	Radio frequency negative permittivity in random carbon nanotubes/alumina nanocomposites. Nanoscale, 2017, 9, 5779-5787.	5.6	157
133	Regulation mechanism of negative permittivity in percolating composites via building blocks. Applied Physics Letters, 2017, 111, .	3.3	72
134	Tunable and weakly negative permittivity in carbon/silicon nitride composites with different carbonizing temperatures. Carbon, 2017, 125, 103-112.	10.3	199
135	Tailorable radio-frequency negative permittivity of titanium nitride sintered with different oxidation pretreatments. Ceramics International, 2017, 43, 16980-16985.	4.8	30
136	C/SiO2 meta-composite: Overcoming the λ/a relationship limitation in metamaterials. Carbon, 2017, 125, 1-8.	10.3	90
137	Flexible polydimethylsiloxane/multi-walled carbon nanotubes membranous metacomposites with negative permittivity. Polymer, 2017, 125, 50-57.	3.8	379
138	Generation mechanism of negative permittivity and Kramers–Kronig relations in BaTiO ₃ /Y ₃ Fe ₅ O ₁₂ multiferroic composites. Journal of Physics Condensed Matter, 2017, 29, 365703.	1.8	31
139	Tunable negative permittivity behavior of random carbon/alumina composites in the radio frequency band. RSC Advances, 2016, 6, 87153-87158.	3.6	28
140	Selectively assembled 2D microarrays from binary nanocrystals. CrystEngComm, 2016, 18, 3008-3014.	2.6	6
141	Ultrahigh dielectric loss of epsilon-negative copper granular composites. Materials Letters, 2016, 169, 86-89.	2.6	26
142	Negative permittivity in Fe–Si–Ni/epoxy magnetic composite materials at high-frequency. Materials Chemistry and Physics, 2016, 170, 113-117.	4.0	11
143	Fabrication and magnetic properties of electrospun cobalt nanofibers. Materials and Design, 2016, 89, 543-548.	7.0	14
144	Negative permittivity behavior in the carbon/silicon nitride composites prepared by impregnation-carbonization approach. Carbon, 2016, 96, 678-684.	10.3	67

#	Article	IF	CITATIONS
145	Large-Area, Low-Cost Infrared Metamaterial Fabrication Via Pulsed Laser Deposition with Metallic Mesh as a Shadow Mask. Plasmonics, 2016, 11, 373-379.	3.4	5
146	Tunable negative permittivity based on phenolic resin and multi-walled carbon nanotubes. RSC Advances, 2015, 5, 16618-16621.	3.6	22
147	Percolative silver/alumina composites with radio frequency dielectric resonance-induced negative permittivity. RSC Advances, 2015, 5, 107307-107312.	3.6	36
148	Negative permittivity behavior in Fe50Ni50/Al2O3 magnetic composite near percolation threshold. Journal of Magnetism and Magnetic Materials, 2015, 381, 105-108.	2.3	29
149	Experimental realization of tunable negative permittivity in percolative Fe ₇₈ Si ₉ B ₁₃ /epoxy composites. RSC Advances, 2015, 5, 9472-9475.	3.6	43
150	Perovskite (La,Sr)MnO3 with tunable electrical properties by the Sr-doping effect. Journal of Alloys and Compounds, 2015, 628, 429-432.	5.5	53
151	Moisture-proof and enhanced effect of inorganic coating on porous Si3N4 ceramic. Journal Wuhan University of Technology, Materials Science Edition, 2015, 30, 311-314.	1.0	4
152	Enhancing the comprehensive electrochemical performance by compositing intercalation/deintercalation-type of TiO2 with conversion-type of MnO. Journal of Alloys and Compounds, 2015, 640, 15-22.	5.5	4
153	Random copper/yttrium iron garnet composites with tunable negative electromagnetic parameters prepared by in situ synthesis. RSC Advances, 2015, 5, 61155-61160.	3.6	49
154	Radio-frequency permeability and permittivity spectra of copper/yttrium iron garnet cermet prepared at low temperatures. Journal of the European Ceramic Society, 2015, 35, 1219-1225.	5.7	56
155	Tunable radio-frequency negative permittivity in nickel-alumina "natural―meta-composites. Applied Physics Letters, 2014, 104, .	3.3	51
156	Spinel ZnMn ₂ O ₄ Nanocrystalâ€Anchored 3D Hierarchical Carbon Aerogel Hybrids as Anode Materials for Lithium Ion Batteries. Advanced Functional Materials, 2014, 24, 4176-4185.	14.9	150
157	3D Interconnected Porous Carbon Aerogels as Sulfur Immobilizers for Sulfur Impregnation for Lithiumâ€Sulfur Batteries with High Rate Capability and Cycling Stability. Advanced Functional Materials, 2014, 24, 2500-2509.	14.9	206
158	Fabrication of luminescent and macroporous Y2O3:Eu3+-coated silica monoliths via freeze drying. Colloids and Surfaces A: Physicochemical and Engineering Aspects, 2014, 441, 481-488.	4.7	5
159	Negative permittivity behavior and magnetic performance of perovskite La _{1â^*x} Sr _x MnO ₃ at high-frequency. Journal of Materials Chemistry C, 2014, 2, 1028-1033.	5.5	88
160	Tunable Electromagnetic Properties in <scp><scp>Co</scp></scp>	3.8	73
161	Ultra low percolation threshold and significantly enhanced permittivity in porous metal–ceramic composites. Journal of Materials Chemistry C, 2014, 2, 6752.	5.5	38
162	Microstructure and dielectric properties of ion-doped La0.7Sr0.3MnO3 lossy ceramics at radio frequencies. RSC Advances, 2014, 4, 25804.	3.6	8

#	Article	IF	CITATIONS
163	Carbon-Coated Fe–Mn–O Composites as Promising Anode Materials for Lithium-Ion Batteries. ACS Applied Materials & Interfaces, 2013, 5, 9470-9477.	8.0	48
164	One-step preparation of a composite consisting of graphene oxide, Prussian blue and chitosan for electrochemical sensing of hydrogen peroxide. Mikrochimica Acta, 2013, 180, 295-301.	5.0	27
165	Preparation of Iron Networks Hosted in Porous Alumina with Tunable Negative Permittivity and Permeability. Advanced Functional Materials, 2013, 23, 4123-4132.	14.9	167
166	Microstructure and metal–dielectric transition behaviour in a percolative Al2O3–Fe composite via selective reduction. RSC Advances, 2013, 3, 26110.	3.6	14
167	Tunable negative permittivity behavior and conductor–insulator transition in dual composites prepared by selective reduction reaction. Journal of Materials Chemistry C, 2013, 1, 79-85.	5.5	39
168	Experimental realization of simultaneous negative permittivity and permeability in Ag/Y3Fe5O12 random composites. Journal of Materials Chemistry C, 2013, 1, 1633.	5.5	80
169	Ordered mesoporous SnO2 with a highly crystalline state as an anode material for lithium ion batteries with enhanced electrochemical performance. CrystEngComm, 2013, 15, 3696.	2.6	50
170	Enhanced Electrochemical Performance of FeWO ₄ by Coating Nitrogen-Doped Carbon. ACS Applied Materials & Interfaces, 2013, 5, 4209-4215.	8.0	47
171	Random Composites of Nickel Networks Supported by Porous Alumina Toward Double Negative Materials. Advanced Materials, 2012, 24, 2349-2352.	21.0	249
172	Highâ€Frequency Negative Permittivity from <scp><scp>Fe/Al</scp>₂<scp>O</scp>₃</scp> Composites with High Metal Contents. Journal of the American Ceramic Society, 2012, 95, 67-70.	3.8	49
173	Preparation and Characterization of α-(Fe, Al)2O3 Solid Solutions by Sol–Gel Method. Journal of Inorganic and Organometallic Polymers and Materials, 2012, 22, 86-89.	3.7	0
174	Magnetic multiresonance behavior of Fe@Al2O3 nanoembedments and microstructural evolution during mechanosynthesis. Journal of Alloys and Compounds, 2011, 509, 5600-5603.	5.5	3
175	Microwave absorption properties of MWCNT-SiC composites synthesized via a low temperature induced reaction. AIP Advances, 2011, 1, .	1.3	23
176	Microwave absorption properties of Fe@Al2O3 nanoembedments prepared by mechanosynthesis. Materials Chemistry and Physics, 2011, 130, 615-618.	4.0	35
177	Synthesis and Characterization of Iron Particles Hosted in Porous Alumina. Journal of Inorganic and Organometallic Polymers and Materials, 2011, 21, 836-840.	3.7	3
178	Lowâ€Temperature Synthesis of Meshy Boron Nitride with a Large Surface Area. European Journal of Inorganic Chemistry, 2010, 2010, 3174-3178.	2.0	14
179	Rapid, Lowâ€Temperature Synthesis of βâ€SiC Nanowires from Si and Graphite. Journal of the American Ceramic Society, 2010, 93, 2415-2418.	3.8	7
180	Carbon Nanotube Reinforced Intermetallic. Advanced Composite Materials, 2010, 19, 261-267.	1.9	7

#	Article	IF	CITATIONS
181	Morphology-controlled ZnO particles from an ionic liquid precursor. CrystEngComm, 2009, 11, 2683.	2.6	21
182	Effect of ECAP pass number on mechanical properties of 2A12 Al alloy. Journal Wuhan University of Technology, Materials Science Edition, 2008, 23, 71-73.	1.0	6
183	Kinetics of thermite reaction in Al-Fe2O3 system. Thermochimica Acta, 2006, 440, 129-131.	2.7	98
184	Fabrication and electrical conductivity of Lu2(Ti1-xHfx)2O7 transparent ceramics prepared by spark plasma sintering. Journal of Asian Ceramic Societies, 0, , 1-9.	2.3	1
185	Effect of Fast Multiple Rotation Rolling on Microstructure and Properties of Ti6Al4V Alloy. Journal of Shanghai Jiaotong University (Science), 0, , 1.	0.9	0